Supporting Information

St-Pierre and Endy 10.1073/pnas.0808831105

SI Text

SI Experimental Procedures. ***Strains and media.*** We obtained *Escherichia coli* strains MG1655 (*F*$^-$*lambda*$^-$*rph-1*) and JW4132 [*F*$^-$*lambda*$^-$*rph-1* Δ(*araD-araB*)567 *lacZ*::*rrnB-3* Δ(*rhaD-rhaB*)568 *hflK*::*kanR*] from the Coli Genetic Stock center. λ$^+$ and λ *c*I26 are originally from the collection of Frank Stahl (University of Oregon, Eugene, OR). λ *c*I857 *bor*::*kanR* was constructed by Lynn Thomason in the laboratory of Donald L. Court (National Cancer Institute-Frederick, Frederick, MD); in this phage, the *kanR* cassette is integrated into the lambda genome as a partial replacement of the *bor* locus, *bor* encodes a lipoprotein expressed in lysogens (1) that is not known to be involved in the lysis-lysogeny decision (see Fig. S2*d* for a comparison of the lysis-lysogeny statistics of λ*c*I857 *bor*::*kanR* to wild-type lambda). Construction of λ *A*am19 *b*::*GFP c*I857 is described in a separate section. Lambda stocks were made by the plate lysis method (2), by using tryptone broth (TB) or LB agar containing various supplements (3). We verified that all our phage stocks produced the expected plaque morphology (clear or turbid) on TB agar plates incubated at 30 °C and 42 °C. Phage titers were performed essentially as described (2). We made plating cells by growing MG1655 in TB supplemented with 0.2% maltose to exponential phase and resuspending them to ≈6E8 cells/mL in TB supplemented with 10 mM $MgSO_4$. TB, agar and soft agar were made as previously described (3). M9GlyM is M9 (3) supplemented with 0.4% glycerol, 0.2% maltose, 2 mM $MgSO_4$ and 0.1 mM $CaCl_2$.

Preparation of stationary phase cells. We grew MG1655 cultures in TB at 37 °C to an OD_{600} of 0.40, as measured by a UV160U spectrophotometer (Shimadzu Scientific Instruments). We diluted the culture 500-fold into 0.5L of TB in a 2.8 L baffled flask, and continued growth with shaking (220 rpm) and aeration for 16 h at 37 °C (Fig. S2*a*).

Preparation of exponential phase cells. We diluted overnight cultures of JW4132 (Coli Genetic Stock Center #10975) in M9GlyM + 10 μg/mL kanamycin and grew them at 30 °C with vigorous shaking to $OD_{600} \approx 0.07$ (UV160U spectrophotometer, see above). We diluted the culture 1,000-fold in fresh M9GlyM supplemented with 1 mM IPTG (to induce GFP expression after infection with *A*am19 *b*::*GFP c*I857) and grew the culture back to $OD_{600} \approx 0.07$.

Counterflow centrifugal elutriation. We fractioned cells according to differences in terminal sedimentation velocity by using a JE5.0 counterflow centrifugal elutriation system equipped with a single 40-mL chamber precooled to 4 °C (Beckman Coulter). Elutriation has been used to isolate fractions of small *E. coli* cells from asynchronous populations (4). Here, we developed protocols to obtain many fractions of *E. coli* cells across a range of mean cell volumes (MCVs).

Elutriation setup. Fig. S3 depicts the critical elements of our setup. We controlled cell and medium flow rate via a peristaltic pump loaded with small pump head cartridges and fitted with L/S14 silicon tubing (Cole-Parmer). We increased fraction quality by using 2 anti-parallel pump heads and a pulse-damping chamber to improve continuity of flow in the elutriation chamber; the damping chamber also trapped small bubbles that otherwise would have disrupted flow within the chamber or caused rotor vibration. We switched the pulse-damping chamber on-line after cell loading by means of a 3-way valve. The list of parts used in our system is given in Table S2.

The air purge system (data not shown) was necessary to remove air from our system before each run. Because we could not achieve the ≈200 mL/min flow rate necessary to purge air from the elutriator by using our elutriation pump, we devised a separate pump system (see Table S2) for the sole purpose of purging air. A 3-way valve was used to control whether the air purge pump or our normal elutriation pump was switched on-line.

We developed 2 elutriation protocols, optimized to isolate smaller and larger MG1655 cells, respectively. During an experiment, we carried out each protocol in parallel by using 2 independent elutriation systems. For both protocols, we first filled the system with an ice-cold solution of 1x M9 salts, purged any air from each elutriation system and brought the rotors to 4800 RPM for at least 15 min before cell loading. We vortexed cells vigorously for 2 min before loading to reduce cell clumping in the elutriation chambers. We then loaded each elutriation system with 120 mL of cells at a flow rate of 3 mL/min. To collect fractions of small MG1655 cells, we kept the flow rate at 3 mL/min for 20 min to allow cells to equilibrate in the chamber. We then increased the flow rate to 4, 5 and then 6 mL/min, collecting 0.5 L at each flow rate. The 6 mL/min fraction contained the smallest cells; therefore, we discarded the other 2 fractions. To collect fractions of larger MG1655 cells, after loading the cells into the elutriator, we slowly increased the flow rate to 7 mL/min. We then increased the flow rate from 7 to 13 mL/min in 1 mL/min steps, collecting 0.5 L at each flow rate. We collected increasing volume cells from the 9, 10, 11, 12 and 13 mL/min fractions (we only collected 0.1 L at the 13 mL/min flow rate). A rough estimate of the amount of cells obtained at each flow rate is presented in Table S1.

We noticed that our protocol to isolate the smallest cells would sometimes lead to complete clogging of the elutriation chamber inflow tube near the bottom (distal) end of the chamber. Such clogging typically occurred within an hour after all cells were loaded in the chamber. We aborted the size-fractionation whenever such clogging occurred. We therefore suggest that users of this method try loading fewer cells, or loading and/or equilibrating cells in the chamber at a slightly higher flow rate, e.g., 4 mL/min.

Electronic and microscopy measurements of cell size from elutriated fractions. We measured the volumes of individual cells in each elutriated fraction (and the starting unfractionated culture) by 2 methods: light microscopy and electronic volume. For microscopy measurements, we spread cells on 0.85% NaCl agarose pads and took pictures by using a TE2000-E inverted microscope equipped with a 60× DM phase contrast objective, 1.5× intermediate magnification (Nikon USA) and an ORCA-AG CCD camera (Hamamatsu Photonics K.K.) controlled by IPLab v3.9 software (BD Biosciences). We manually measured the long axis of >500 cells per fraction. We converted cell length measurements (pixels) to absolute length (microns) by using a calibration slide (AppliedPrecision). We converted measured cell lengths to cell volumes by modeling cells as hemisphere-capped cylinders: Cell volume = $4/3\pi r^3 + (L\text{-}2r)\pi r^2$, where L is the cell length and r is half the cell diameter. r was assumed to be identical (0.44 μm) for all cells. We chose this value of r by measuring the mean cell diameter of >500 cells from an asynchronous MG1655 population grown as described above. We did not take into account cell–cell differences in cell width in our measurements of volume because we did not feel they were accurate, in part because the standard deviation in width measurement (≈0.14 μm) is smaller than the optical resolution (≈0.2 μm) of our system.

To obtain electronic volume measurements, we used an NPE

Cell Quanta Hg/488 equipped with 25-μm flow chamber (NPE Systems) (5). To better separate cell volume measurements from electronic noise, we stained cells with Syto-9 (Invitrogen) and triggered on fluorescence rather than volume. For staining, we first diluted cells to ≈1E6 cells/mL in NPE isodiluent (NPE Systems) and incubated with 2 μM Syto-9 for 30 min at 4 °C in the dark. We calibrated our electronic volume measurements by spiking cell suspensions with 1.51-μm yellow-green fluorescent polystyrene beads (Excitation: 425 nm, Emission: 480 nm; Catalog No. FS04F, Bangs Labs). Cells and beads were excited with a 488-nm laser and their emission monitored by using a 525/30-nm emission filter. Electronic volume (gain setting = 10) and fluorescence were recorded for >10,000 cells and 5,000 beads per fraction. Electronic and microscopy measurements gave similar values of mean cell volume (Fig. S10).

Quantification of developmental outcomes by using macroscopic plate tests. We measured developmental outcomes by using a lambda phage engineered to confer kanamycin resistance in lysogenic cells and to only produce lytic cells at temperatures >40 °C (λ *c*I857 *bor*::*kanR*). We confirmed unsorted population statistics by using wild-type lambda (λ^+). To measure cell fate outcomes we first resuspended cells to 1E9 cells/mL in ice-cold TB supplemented with 10 mM $MgSO_4$. We added phage at an average phage to cell ratio of 0.005 (λ *c*I857 *bor*::*kanR*) or 0.05 (λ^+). We incubated cell-phage mixtures at 4 °C for 30 min to allow for adsorption. Adsorption was not significantly affected by cell size (Fig. S6*b*). We removed unadsorbed phage by centrifugation. We then diluted cells 10-fold in TB supplemented with 1 mM $MgSO_4$ prewarmed to 30 °C. We then incubated cells at 30 °C with shaking and aeration for 45 min, after which we placed cultures on ice; this incubation step is necessary to allow newly lysogenic cells to develop kanamycin resistance (λ *c*I857 *bor*::*kanR*) or superinfection homoimmunity (λ^+). We removed any remaining unadsorbed phage by a final centrifugation step.

We independently measured lysis, lysogeny, and total infected cells. We measured the number of lytic cells by plating cells on TB agar plates containing ≈6E7 plating cells, incubating at 30 °C, and counting plaque forming units (PFU). For experiments using λ *c*I857 *bor*::*kanR*, we measured the number of lysogenic cells by spreading cells on TB agar supplemented with 20 μg/mL kanamycin sulfate. When plating uninfected cells on kanamycin agar, we usually obtained no false positives; in a few cases, up to 0.001% of plated cells gave false positives (data not shown). For experiments using λ^+, we measured the number of lysogenic cells by spreading on TB agar seeded with ≈1E9 λ*c*I26, a lambda mutant that kills any nonlysogenic cells. When plating uninfected cells on λ*c*I26-seeded agar, ≈0.01% of cells produced colonies (false positives). For both λ^+ and λ *c*I857 *bor*::*kanR*, we incubated plates at 30 °C and scored lysogens by counting the number of colony forming units (CFU). For cells infected with λ *c*I857 *bor*::*kanR*, we independently measured the total number of infected cells by preparing plates as if to count lytic events, with the exception that the plates were incubated at 42 °C. At 42 °C, the temperature-sensitive lambda repressor *c*I857 is inactive, so all infected cells select the lytic pathway and can be counted as PFU.

Construction of* λ *Aam19* b::GFP *cI857. We constructed λ *A*am19 *b*::*GFP cI*857 by first recombineering a GFP cassette into wild-type lambda using published methods (6). The *GFP* cassette was PCR-amplified from part BBa_I20115 (7) in plasmid vector pSB3K3 (7). It contains GFP variant BBa_E0040 (7) under the control of an LacI-repressible promoter (BBa_R0011) (7), as well as a kanamycin marker to select recombinants. The primers used for amplification contained 20 bp of homology to the *GFP* cassette and 48–50bp of homology to lambda *b* region: forward primer, aggcagcaaaatcatcagaaacgaacgcatcatcaagtgccggtcgtgcaaactttatccgcctccatcc; reverse primer, ccgtatccttcacccaggctgtgccgttccacttctgatattcccctcccgtgaagaaggtgttgctga.

We used ethanol purification to desalt and concentrate our PCR product, and performed membrane dialysis for further desalting. We performed recombineering on an infectious lambda wild-type particle by using the recombineering strain DY380 and published methods (6). To select for recombinants, we infected MG1655 cells grown to stationary phase with the recombineering lysate and plated on LB supplemented with 20 μg/mL kanamycin. Putative λ *b*::*GFP* lysogens were confirmed by PCR and fluorescence microscopy. Stocks of λ *b*::*GFP* were derived from these lysogens by using standard methods (8). The resulting phage contained our 2,662-nt *GFP* cassette into the *b* region (9) of the phage genome, replacing sequence between lambda coordinates 20430–22278 and producing a phage only slightly longer (813 nt or 1.7%) longer than wild-type λ. We confirmed the presence of the cassette by fluorescence microscopy and by sequencing.

We next engineered the *A*am19 (C→T at lambda coordinate 1917) and *c*I857 (C→T at lambda coordinate 37742) mutations onto λ *b*::*GFP* by using published methods of recombineering using single stranded oligonucleotides (6, 10). Note that the *c*I857 mutation was introduced onto λ *b*::*GFP* to allow a simpler detection of *A*am19 mutants. We identified recombinants by plaque morphology and confirmed the presence of the mutations by sequencing.

Single-cell time-lapse microscopy. *Condition 1: MG1655 grown to stationary phase in TB.* We grew MG1655 to stationary phase as for elutriation experiments (see above), resuspended cells in TB + 10 mM $MgSO_4$, and added λ *A*am19 *b*::*GFP c*I857 at a phage-to-cell ratio of ≈1:30. After 30 min at 4 °C for adsorption of phage onto cells, we removed unadsorbed phage by centrifugation and we spread cells on TB + 1 mM IPTG + 2% low melting point (LMP) agarose pads. IPTG was added to induce GFP expression from the GFP cassette encoded on λ *A*am19 *b*::*GFP cI*857. We incubated the cells in a microscope heating chamber set to 30 °C, taking phase contrast and GFP fluorescence images (75 ms) every ≈15 min for at least 9 h at 60–100× magnification.

Condition 2: JW4132 grown to exponential phase in M9-based medium. We grew JW4132 to exponential phase as described above. We concentrated the cells 10-fold in TM (10 mM Tris-Cl, pH 7.5, 10 mM $MgSO_4$) and infected cells with λ *A*am19 *b*::*GFP c*I857 at a phage:cell ratio of ≈1:30. After 30 min at 4 °C for adsorption of phage onto cells, we removed unadsorbed phage by centrifugation and we spread cells on M9GlyM + 1 mM IPTG + 2% LMP agarose pads. We incubated the cells in a microscope heating chamber set to 30 °C, taking phase contrast and GFP fluorescence images (75 ms) every ≈15 min for at least 11 h at 60–100× magnification.

Volume measurements. We identified infected cells by using GFP fluorescence produced by our specialized lambda strain. We manually measured the lengths of individual infected cells by using the first frame of our time-lapse movies and converted those length measurements into volume measurements (in μm^3) as described earlier (see *Electronic and microscopy measurements of cell size from elutriated fractions*). For exponentially growing JW4132, we used a cell diameter of 0.92 μm (instead of 0.88 μm for stationary phase cells) in our calculations of volume; 0.92 μm corresponds to the average diameter measured manually from >300 cells.

SI Results. Additional controls support our claim that variability present before infection controls the fate of lambda infected cells. We tested whether observed differences in cell fate statistics (Fig. 3) were an artifact of the methods we used to sort cells or to measure developmental outcome. To start, we tested whether elutration may have affected cellular physiology in such a way that it grossly influenced the lysis/lysogeny decision. To do this, we performed elutriation by using the described methods

except that elutriated cells were continuously pumped back into the system. Cells that underwent elutriation in this way exhibited the same developmental statistics as cells from the same culture that were not loaded into our elutriation systems (Fig. S6*a*). Next, we tested whether our results might be because of differences in the number of dead or nongrowing cells across the different fractions used. To do this, we followed via microscopy >250 cells from both a low MCV fraction (0.83 μm^3 MCV; 71.5% lysogeny) and a high MCV fraction (1.26 μm^3 MCV; 24.9% lysogeny). In both cases >98% of observed cells grew and divided.

We performed our experiments at an average phage-to-cell ratio of 0.005 to ensure that virtually all infected cells (≈99.8%) were infected at an MOI = 1. However, infection of larger cells could have resulted in lower percentage lysogeny not because more large cells opted for lytic growth, but because lysogeny may not have proceeded to completion. For example, larger cells may be more sensitive to kanamycin, resulting in an underestimation of percentage lysogeny when large cells are plated on kanamycin agar. However, if this occurred, the sum of independent measurements of lysogens and lytic centers would likely not have equaled the independent measurements of the total number of infected cells (Fig. 3). Moreover, we saw no difference in frequency of lysogenization when a different method was used to select lysogens after infection of an asynchronous population of cells (e.g., Fig. S2*c*). Our results are also unlikely to be an artifact of the particular genotype of the phage used in our experiments (λ *c*I857 *bor*::*kanR*), as both wt λ and λ *c*I857 *bor*::*kanR* produced identical frequencies of lysogeny after infection of an asynchronous population of stationary phase cells (Fig. S2*d*).

Finally, since cells were incubated for 45 min at 30 °C in liquid medium between phage adsorption and plating (above), cell division or lysis could have occurred during this period, potentially skewing the developmental outcome statistics. However, we found no increase in colony or plaque counts during this incubation period for uninfected or infected fractions at both high and low MCV, respectively (Fig. S6 *c* and *d*). We confirmed the absence of cell division by using time-lapse microscopy (data not shown). This lag in cell division may result from our use of stationary phase cells.

1. Barondess JJ, Beckwith J (1995) Bor gene of phage lambda, involved in serum resistance, encodes a widely conserved outer membrane lipoprotein. *J Bacteriol* 177:1247–1253.
2. Ausubel FM, *et al.*, eds (2001) *Current protocols in molecular biology* (Wiley, New York).
3. Sambrook J, Russell DW (2001) *Molecular Cloning: A laboratory manual* (Cold Spring Harbor Lab Press, Cold Spring Harbor, NY).
4. Figdor CG, Olijhoek AJM, Klencke S, Nanninga N, Bont WS (1981) Isolation of small cells from an exponential growing culture of Escherichia coli by centrifugal elutriation. *FEMS Microbiol Lett* 10:349–352.
5. Thomas RA, Krishan A, Brochu M (2002) High resolution flow cytometric analysis of electronic nuclear volume and DNA content in normal and abnormal human tissue. *Methods Cell Sci* 24:11–18.
6. Thomason L, *et al.* (2007) Recombineering: Genetic engineering in bacteria using homologous recombination. *Curr Protoc Mol Biol* Chapter 1:Unit 1.16.
7. Registry of Standard Biological Parts, http://partsregistry.org.
8. Hendrix RW (1983) *Lambda II* (Cold Spring Harbor Lab Press, Cold Spring Harbor, NY), pp 693.
9. Court D, Oppenheim AB (1983) *Lambda II*, eds Hendrix RW, Roberts JW, Stahl FW, Weisberg RA (Cold Spring Harbor Lab Press, Cold Spring Harbor, NY), pp 251–277.
10. Oppenheim AB, Rattray AJ, Bubunenko M, Thomason LC, Court DL (2004) In vivo recombineering of bacteriophage lambda by PCR fragments and single-strand oligonucleotides. *Virology* 319:185–189.
11. Wahl AF, Donaldson KL (2001) *Current Protocols in Cell Biology*, ed Bonifacino JS (Wiley, New York).
12. Mackay DJ, Bode VC (1976) Events in lambda injection between phage adsorption and DNA entry. *Virology* 72:154–166.
13. Shetty RP, Endy D, Knight TF, Jr. (2008) Engineering BioBrick vectors from BioBrick parts. *J Biol Eng* 2:5.

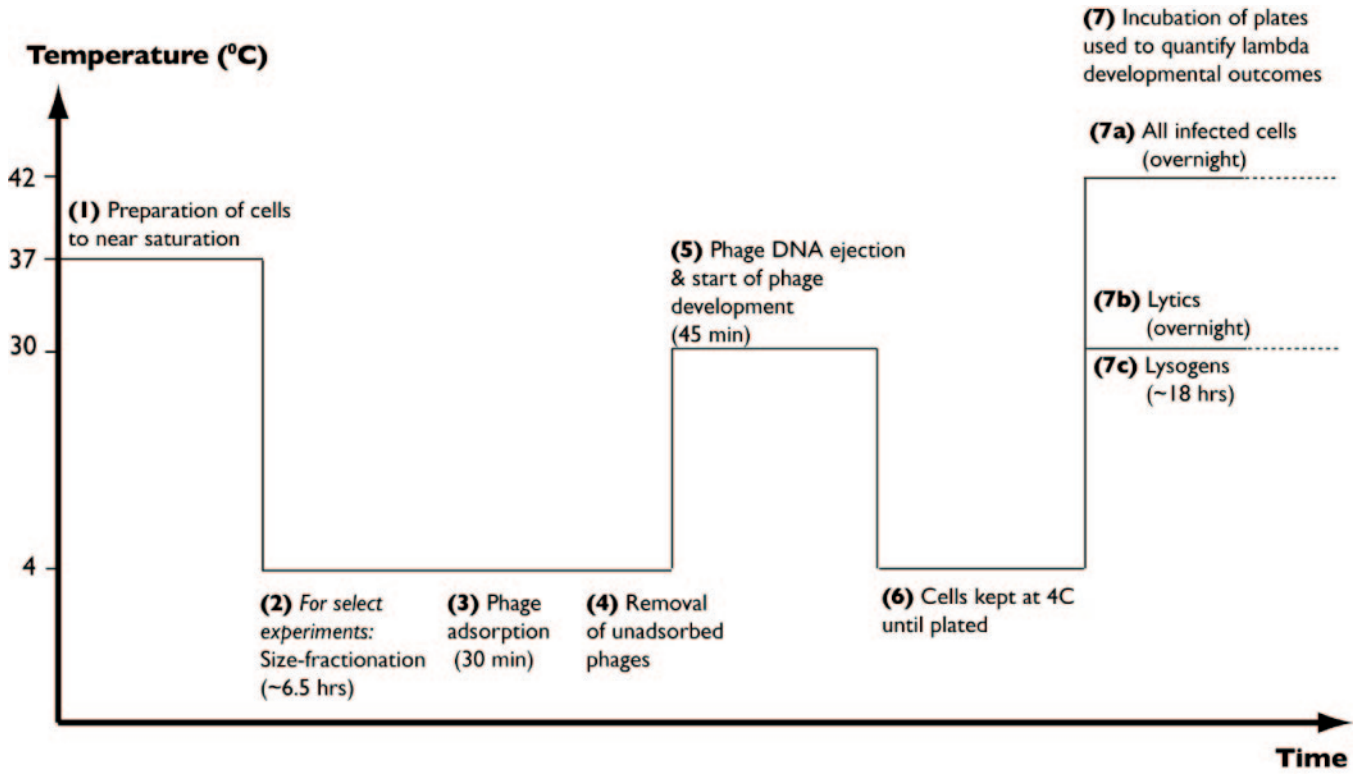

Fig. S1. Sketch of experimental procedure. The major steps of the experimental protocols are shown. The duration of the steps is indicated where appropriate.

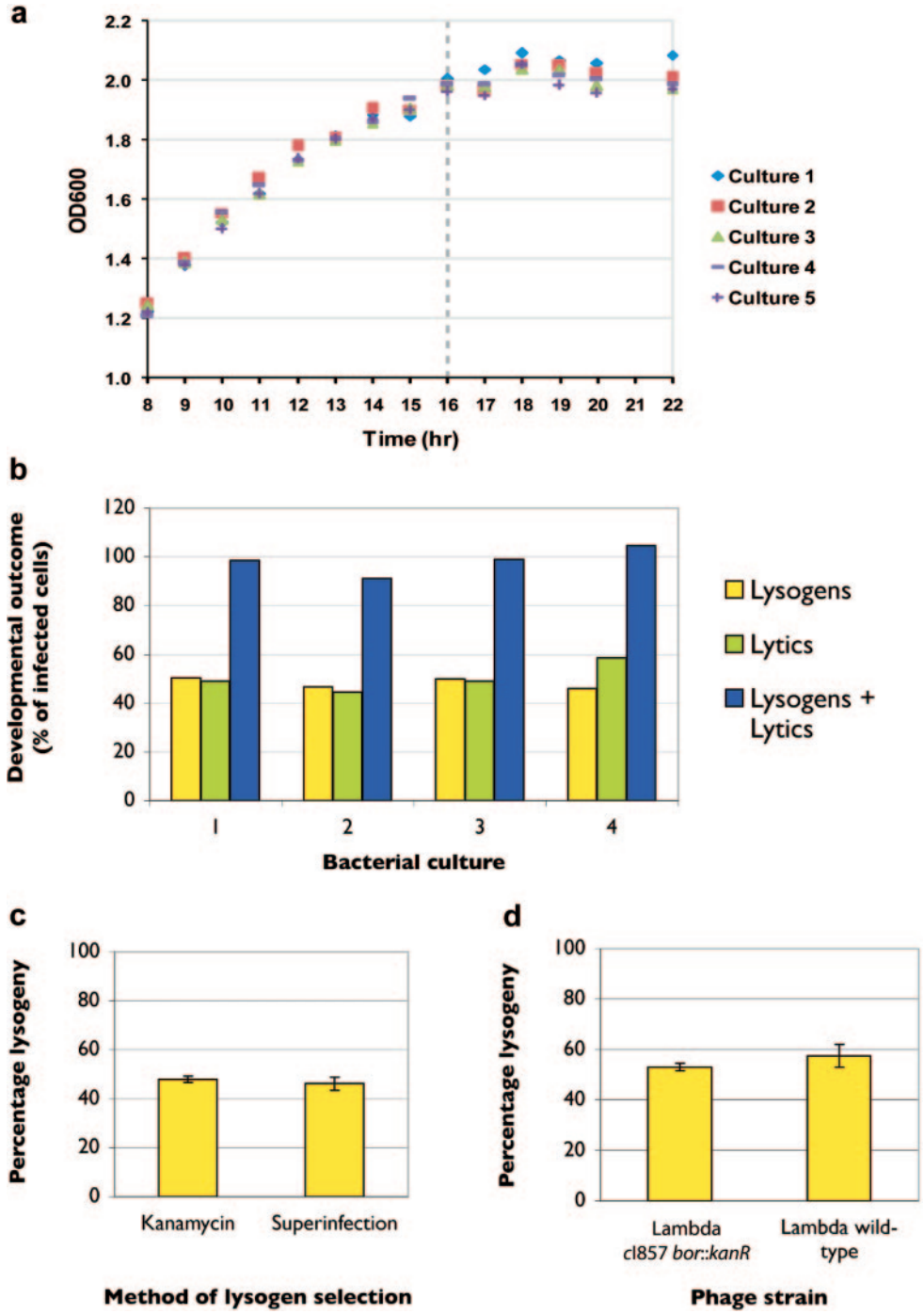

Fig. S2. Genetically identical cells, each infected with a single phage, can produce distinct developmental outcomes. (*a*) We grew 5 cultures of *Escherichia coli* MG1655 from independent colonies as described in *SI Text*. Aliquots from each culture were diluted 3-fold into TB for OD_{600} measurement via a Shimatzu UV160U spectrophotometer (Shimadzu Scientific Instruments). The time represents the number of hours after the 500-fold dilution in 0.5L TB (see *SI Experimental Procedures*). The dotted line indicates when we would normally harvest cells for size fractionation and/or infection (i.e., 16 h after dilution). Dilution and time-independent measurement error was determined by comparing the OD_{600} readings of 10 separate 3-fold dilutions of stationary phase cells. The coefficient of variation of those measurements was $<1\%$. (*b*) Four independent infected cultures produce similar fractions of lytic and lysogenic outcomes, the sum of which equals an independent measure of total infected cells. (*c*) Population-wide cell fate statistics are insensitive to the method of lysogeny quantitation. The error bars represent the standard error of the mean of 3 infections made with independent stocks of λ cI857 *bor*::*kanR*. (*d*) A culture of stationary phase cells was infected with 3 independent stocks of λ^+ and 3 independent stocks of λ cI857 *bor*::*kanR*. The percentage lysogeny is the number of lysogens over the total number of infected cells (here calculated as the sum of lysogens and lytic events). The error bars represent the standard error of the mean of infections made with 3 independent stocks of λ cI857 *bor*::*kanR* or λ^+.

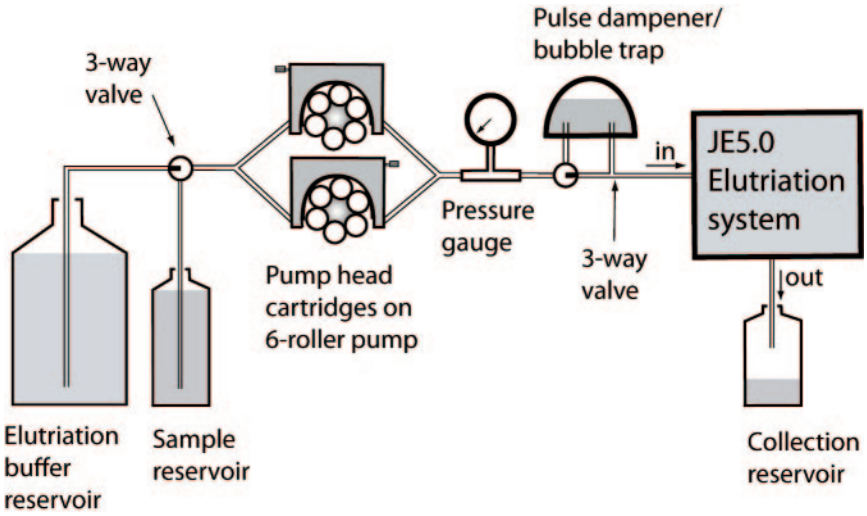

Fig. S3. Schematic of the counterflow centrifugal elutriation system. Our setup was inspired by ref. 11 and the JE5.0 elutriation system instruction manual and is described in *SI Text*.

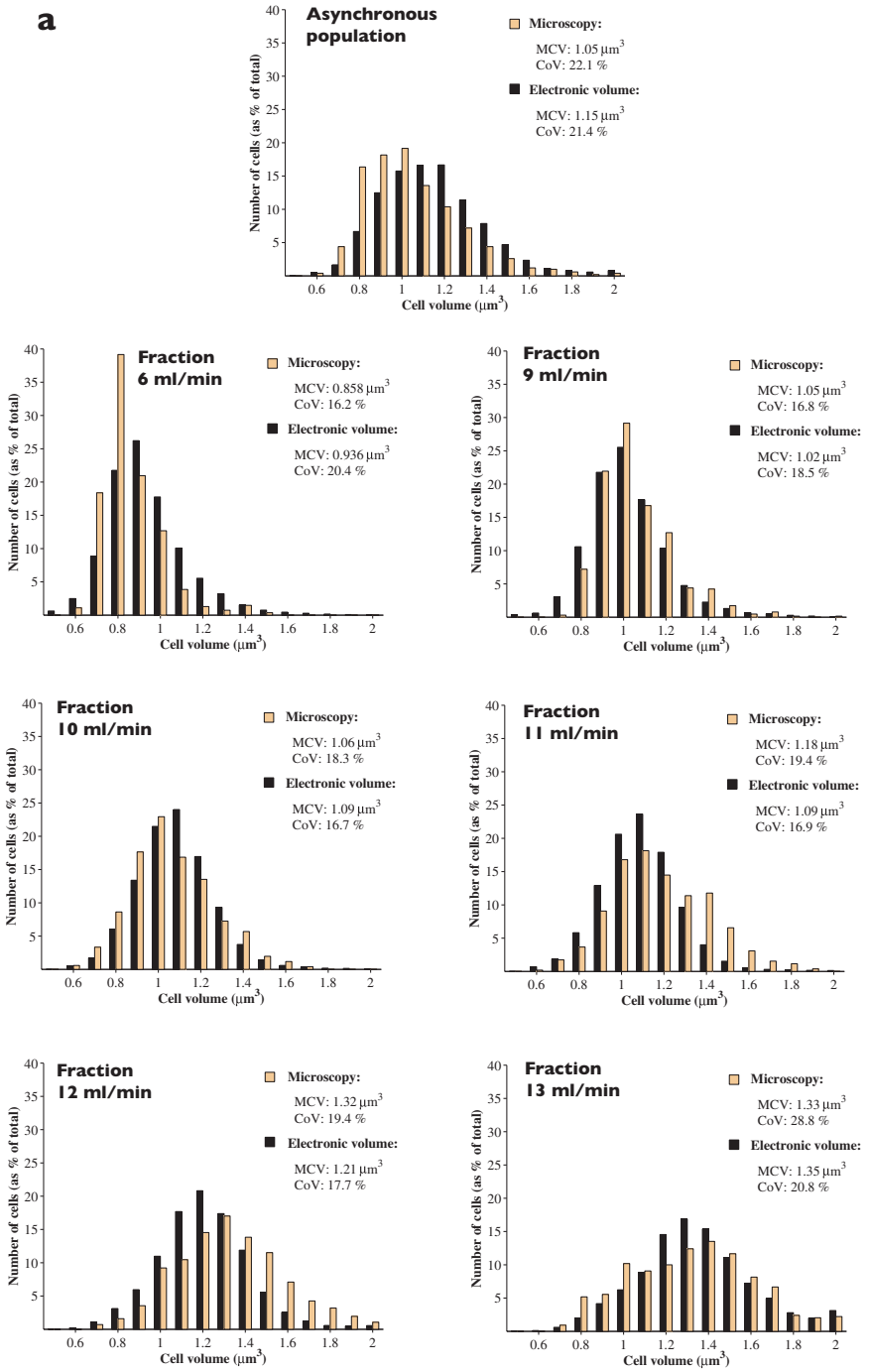

Fig. S4. Volume histograms of elutriated fractions. We plotted volume histograms of all elutriated fractions presented in Fig. 3, as well as the starting asynchronous populations from which they are derived. Set *a* corresponds to the square series of Fig. 3, *b* to the triangle series and *c* to the circle series. For each fraction, we noted the flow rate at which the fraction was obtained, as well as the mean cell volume (MCV) and coefficient of variation (CoV) of the volume distributions measured by microscopy or electronically. Note that during initial loading of cells in the elutriation chamber, we typically get a pellet in the elutriation chamber near in the inflow tube. This pellet contains cells of various volumes. Cells can detach from this pellet during the elutriation procedure, and we believe this is one of the reasons why we obtain small cells in our large cell fractions. Detachment of cells from this pellet may be the reason why in *c*, the 2 fractions collected at the highest flow rates had a lower MCV than the fraction collected at 11 mL/min. We do not have an explanation as to why this occurred in the experiment presented in *c*, but not those of *a* and *b*. Perhaps it is because of small differences in pump calibration between the 3 experiments.

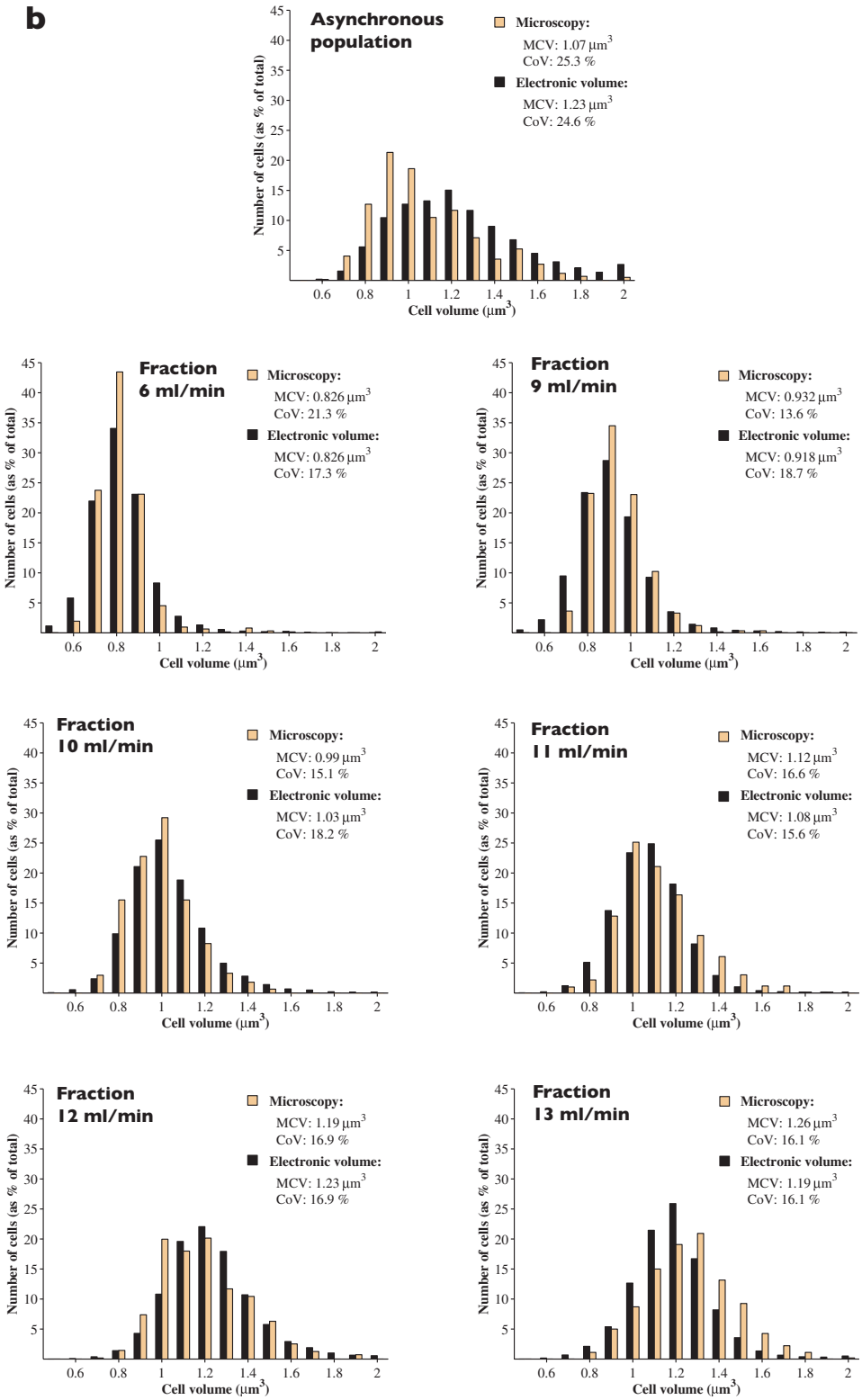

Fig. S4. continued.

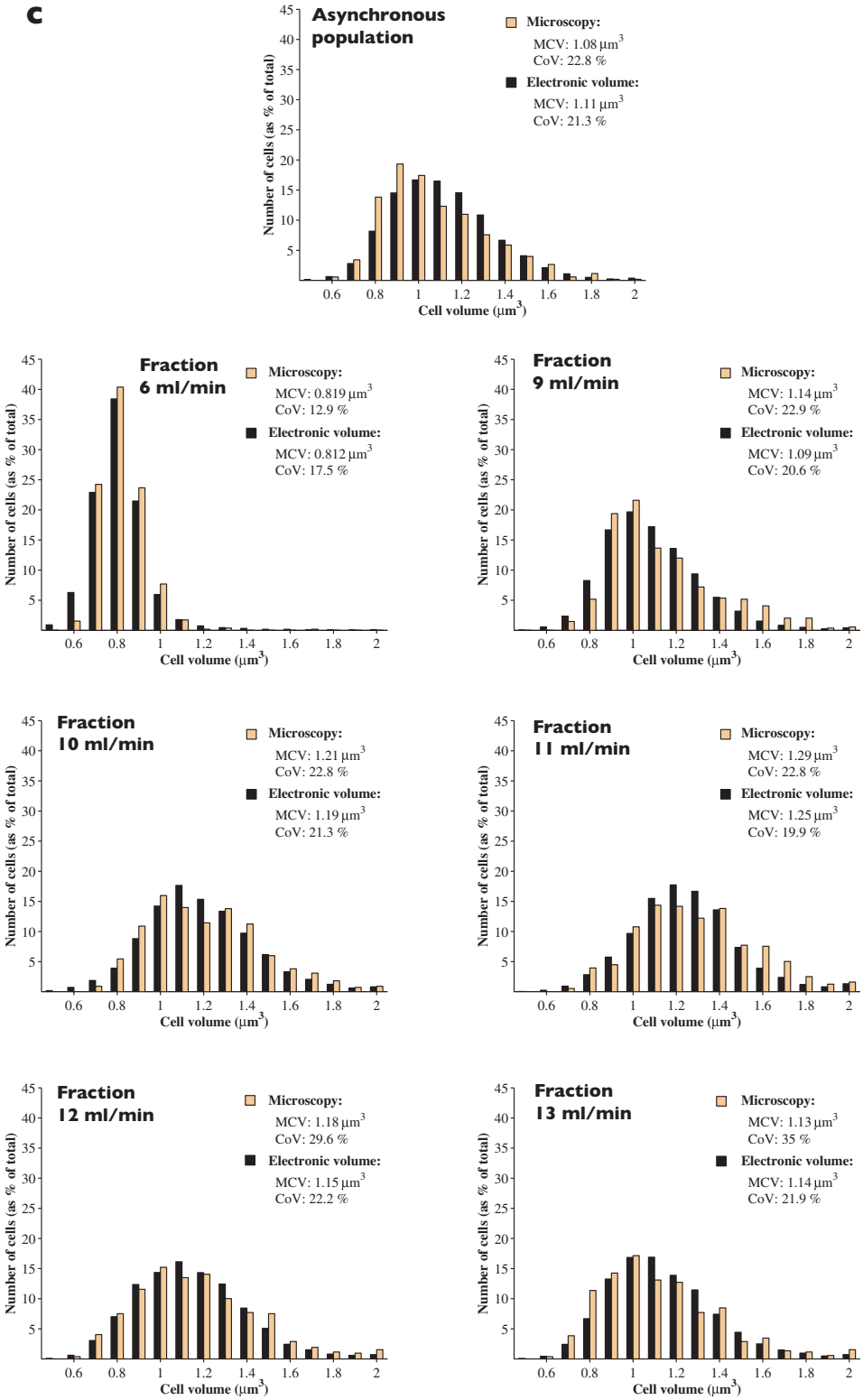

Fig. S4. continued.

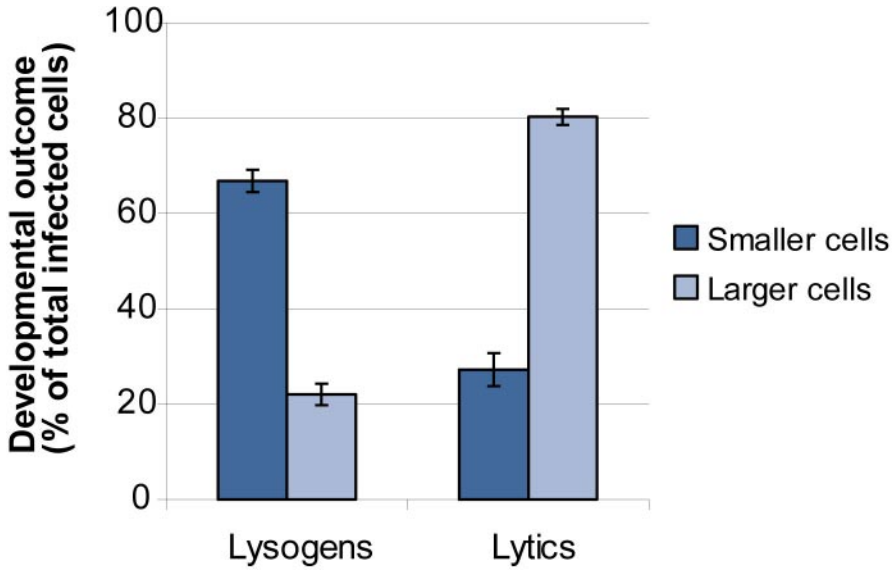

Fig. S5. Comparison of developmental statistics between fractions of infected cells. From the fractions illustrated in Fig. 3 (main text), we further analyzed 3 small MCV fractions and 3 large MCV fractions. Each group was composed of fractions obtained from independent cultures. The small MCV fractions gave an average of 66.8% lysogeny, >3 times the percentage lysogeny observed in the large MCV fractions, 22.0% ($P = 0.002$, 2-tail paired t test). The same fractions gave a corresponding change in frequency of lytic events: We observed 27.3% lytic events in the small MCV fractions compared with 80.3% in the large MCV fractions ($P = 0.003$, 2-tail paired t test). The error bars represent the standard error of the mean of 3 independent fractions.

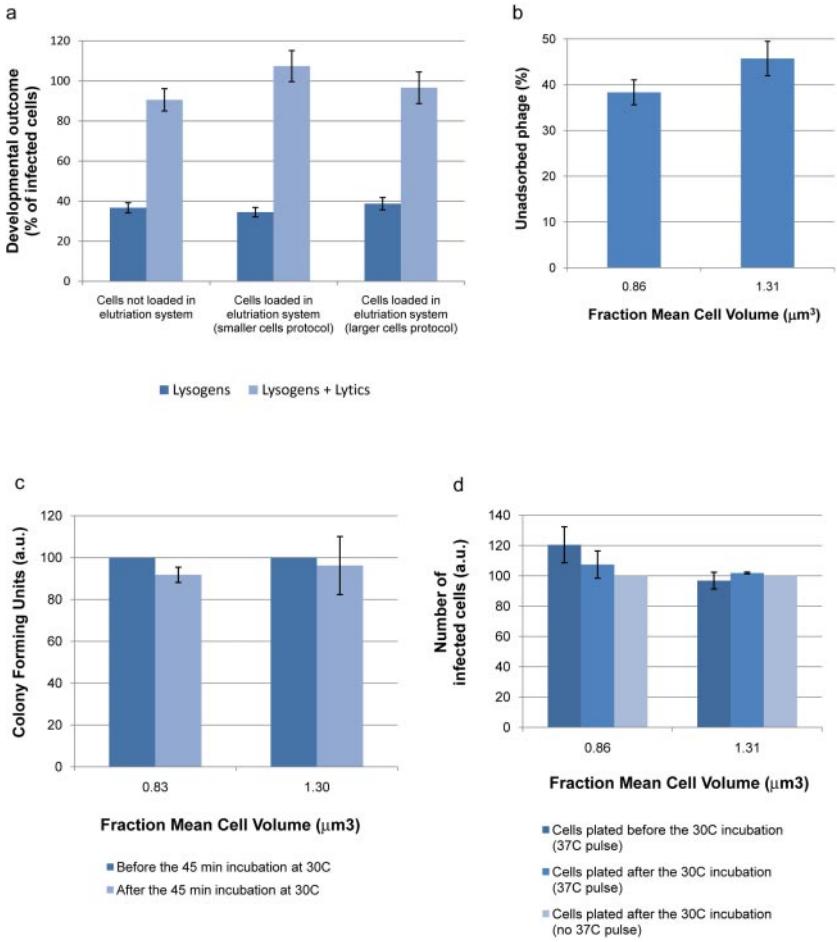

Fig. S6. Various control experiments in support of the claim that host volume is a predictor of the fate of lambda infected cells. (*a*) Counterflow centrifugal elutriation does not result in qualitative changes in developmental outcome statistics of lambda-infected cells. To investigate the effect of our elutriation protocols on lambda development, we modified our elutriation setup so that elutriated cells would be continuously reintroduced into the system. To do this, we made 2 changes to the setup depicted in Fig. S3 and described in *SI Text*. First, the sample reservoir was the only reservoir used. The outflow of the system, including elutriated cells, was collected into the sample reservoir so that it could then be pumped back into the system. Second, the pulse dampener was not used to avoid cells accumulating in its chamber. This setup was used for both elutriation systems, and the 2 protocols described in *SI Text* were followed in parallel. At the end of the procedure, cells were collected into separate containers by using a high flow rate (>20 mL/min) to wash out the cells, and manual removal of the cell pellet that usually forms at the distal end of the elutriation chamber. Cells loaded in the 2 elutriation systems, as well as cells from the same population but not loaded in either of the elutriation systems, were infected with phage lambda and their developmental outcomes quantified. The error bars represent the Poisson error of plating. (*b*) Adsorption of λ cI857 *bor*::*kanR* on high MCV and low MCV fractions is nearly identical. A culture of stationary phase cells was size-fractioned via counterflow centrifugal elutriation as described earlier. The fraction with the largest MCV and the fraction with the smallest MCV were infected with λ cI857 *bor*::*kanR*. After 30-min adsorption at 4 °C, cells were pelleted by centrifugation, and the supernatant titered for unadsorbed phages. The percentage of unadsorbed phages was expressed as the number of unadsorbed phages over the number of input phages. The error bars represent the standard error of the mean of 3 replicate experiments performed by using cells from the same fraction. (*c*) The total number of cells does not increase during the 45-min incubation step between adsorption and plating. We grew and size-fractionated 3 independent cultures of bacterial cells. For each culture, we selected the fraction with the smallest MCV and the fraction with the largest MCV. To replicate experimental conditions of our usual infection protocol (except for the addition of phages), we resuspended cells in TB supplemented with 10 mM $MgSO_4$, incubated them at 4 °C for 30 min and diluted them in TB prewarmed to 30 °C. Cells were then plated on TB agar either immediately after dilution, or after a 45-min incubation at 30 °C with aeration in a roller drum. Plates were incubated at 30 °C for ≈18 h and scored for colony forming units (CFUs). For each experiment and each fraction, the number of CFUs obtained after the 45-min incubation period was normalized to the value obtained when cells were plated before incubation. The error bars represent the standard error of the mean of those 3 independent experiments. The values given for the mean cell volume represent the mean of the MCV of 3 fractions. (*d*) The total number of infected cells does not change during the incubation step between adsorption and plating. We grew and size-fractionated a culture of bacterial cells. The fraction with the largest MCV and the fraction with the smallest MCV were infected with λ cI857 *bor*::*kanR*. After the usual adsorption step (30 min, 4 °C), cells from each fraction were split into 3 treatment groups. Some cells were submitted to a 5-min pulse at 37 °C and plated either immediately (Condition A), or after the usual 45-min incubation at 30 °C (Condition B). The 37 °C pulse was performed to ensure phage DNA ejection before plating (12), thus avoiding potential effects of plating conditions on ejection probability. Cell treated exactly as described in *SI Text* (i.e., 45-min incubation at 30 °C but no 5-min pulse at 37 °C) were also plated (Condition C). Infected cells were scored as plaque forming units (PFUs) on plates incubated at 42 °C. The error bars represent the standard error of the mean of 3 replicate experiments performed by using cells from the same fraction. For each replicate experiment, the number of PFUs obtained in Conditions A and B were normalized to the number of PFUs obtained from Condition C.

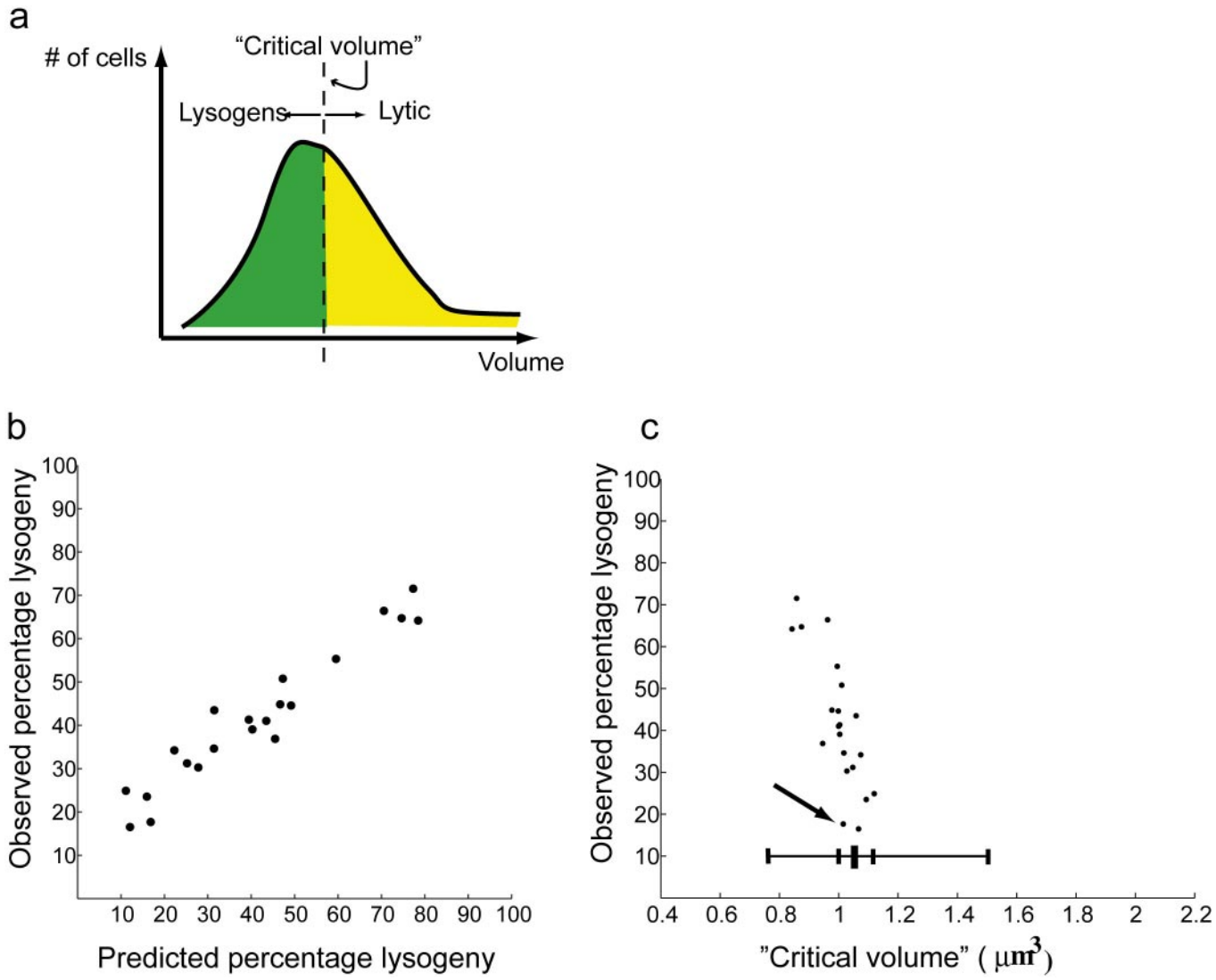

Fig. S7. Critical volume estimates for individual cell fractions (data points). (*a*) We posited a single parameter abstract all-or-none model to posit that any cells smaller than a critical volume might produce a lysogen, whereas any larger cell would undergo lysis. (*b*) We then used this critical volume model to analyze data obtained by elutriation and plating. Specifically, we compared the observed frequency of lysogeny to the frequency of lysogeny that would be predicted using the all-or-none model, fitting for the best critical volume across all cell fractions. The best-fit critical volume model (1.04 μm^3) is a good predictor ($r^2 = 0.93$, $P <$ 1E-04) of observed cell fate. (*c*) For comparison, we also calculated a critical volume for each fraction independently by determining the volume at which the percentage of cells of lesser volume is equal to the observed probability of lysogeny in that fraction. For example, the observed percentage lysogeny for the indicated fraction (arrow) is 17.7%, and the critical volume for this fraction is determined as the volume for which 17.7% of the cells are of lesser volume (1.02 μm^3). From this complementary analysis we observed that the critical volumes across all MCV fractions were concentrated within a range of cell volumes that are much narrower than the volume distribution of the starting asynchronous population, which is indicated by the horizontal bar (center dash represents the mean, 10% of the population fall within the inner dashes, and 90% within the outer dashes). Most critical volume points fall within the inner dashes. To be clear, our mathematical analysis does not conclusively establish a critical volume all-or-none model, nor reveal anything about molecular mechanisms that would underlie such behavior.

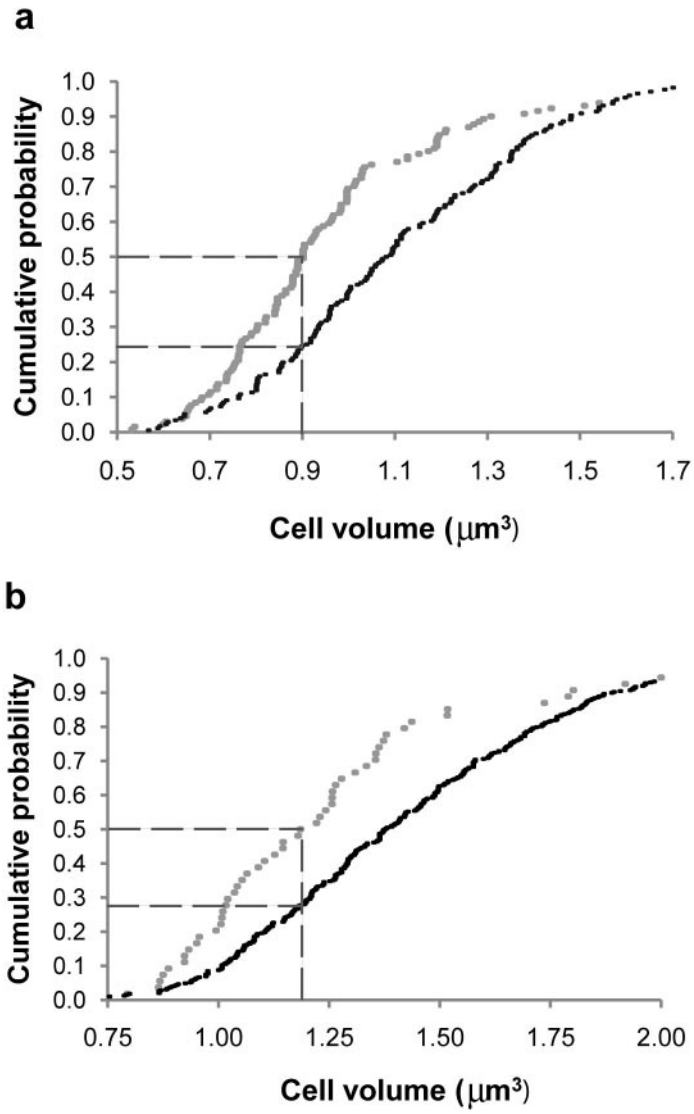

Fig. S8. Cumulative distribution functions (CDF) of cell volume for lytics and lysogens. Probability that individual lysogenic or lytic cells were less than or equal to a given cell length at the start of infection for stationary phase MG1655 in TB (*a*) or exponential phase JW4132 in M9GlyM (*b*). Each dot represents a single cell. In both cases, the cell size of lysogens (gray dots) and lytics (black dots) spanned a similar range, suggesting there is no critical volume (see Fig. S7) below which all cells become lysogens and above which all cells produce lytic events (also see Fig. 5). However, lysogens are overall smaller than lytics. For example, we observed that in individual stationary phase cells, the smallest 50% of cells that became lysogens were $<0.9\ \mu m^3$ whereas only the smallest $\approx$23% of lytics were below this length (*a*, dashed lines). Similarly, in individual exponential phase cells, the smallest 50% of cells that became lysogens were $<1.2\ \mu m^3$ whereas only the smallest $\approx$28% of lytic cells were below this length (*b*, dashed lines).

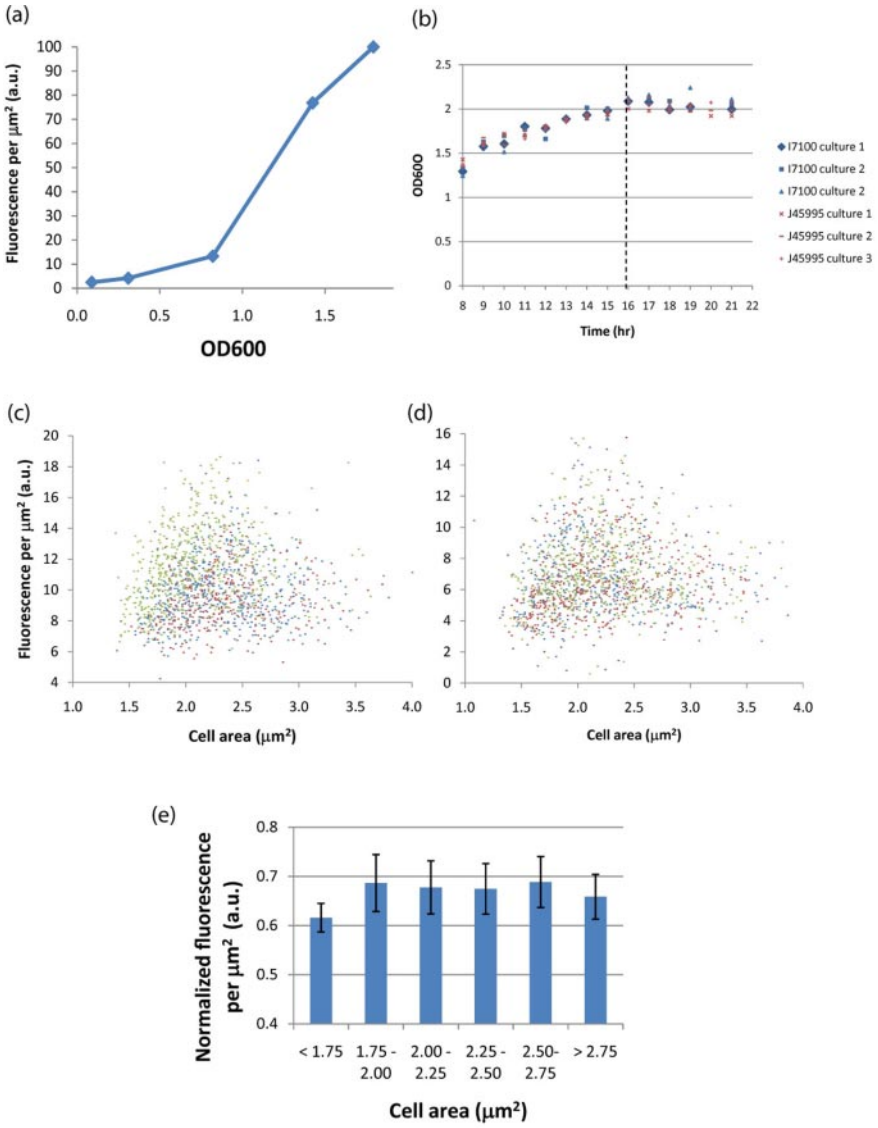

Fig. S9. Cell volume is not correlated with a fluorescent reporter of stationary phase stress. We used BBa_J45995 (7), an existing GFP reporter of stationary phase stress where the promoter of *osmY* is placed upstream of GFP. This reporter was ported to the low-copy vector pSB4K5 (7, 13) and the resulting plasmid (pSB4K5-J45995) transformed into MG1655. As a control, we also used a construct [BBa_I7100, (7)] with the constitutive promoter BBa_R0040 (7) upstream of GFP. I7100 was also ported into pSB4K5. The resulting plasmid (pSB4K5-I7100) was also transformed into MG1655. (*a*) pSB4K5-J45995 becomes more active as cells progress toward stationary phase. We grew 3 independent cultures of MG1655 carrying pSB4K5-J45995 in TB + 10 μg/ml kanamycin sulfate to stationary phase (see *SI Text*). At different points during growth, we spread cells on M9 agarose (2%) pads and imaged at least 300 cells per culture by using phase contrast and fluorescence (50-ms exposure) microscopy. Cell size (as area on the still pictures) and fluorescence were extracted by custom Matlab (Mathworks) scripts. Fluorescence per μm^2 increases with OD_{600}, as expected for a reporter of stationary phase. On the other hand, pSB4K5-I7100 was brightly fluorescent in both exponential and stationary phase (data not shown). (*b*) pSB4K5 reporter plasmids do not significantly change cell growth kinetics and cell fate decision statistics. We grew 3 independent cultures of (*i*) MG1655 carrying pSB4K5-J45995 and (*ii*) MG1655 carrying pSB4K5-I7100 in TB + 10 μg/ml kanamycin sulfate to stationary phase. Aliquots from each culture were diluted 3-fold into TB for OD_{600} measurement via a Shimatzu UV160U spectrophotometer (Shimadzu Scientific Instruments). The time represents the number of hours after the 500-fold dilution in 0.5L TB (see *SI Text*). All cultures reached a plateau in OD_{600} at $\approx$16 h after the start of the culture (dashed line), as was obtained with plasmid-free MG1655 (Fig. S2*a*). pSB4K5-J45995 also did not affect cell fate decision statistics: Infection of stationary phase MG1655 cells carrying pSB4K5-J45995 gave 50.8 $\pm$ 1.0% (n = 3, SEM) lysogeny, compared with 48.9 $\pm$ 2.6% (n = 3, SEM) for plasmid-free MG1655. (*c*–*e*) We observed no correlation between cell size and fluorescence from our stationary phase reporter. Three independent cultures of MG1655/pSB4K5-J45995 and MG1655/pSB4K5-I7100 were grown to stationary phase, imaged and analyzed as described above, with the exception that fluorescence exposure time was lowered to 10 ms for MG1655/pSB4K5-I7100 cells. We plot the fluorescent per μm^2 as a function of cell size for MG1655/pSB4K5-I7100 (*c*) and MG1655/pSB4K5-J45995 (*d*). Cell size is given as the area (in μm^2) covered by each cell on our 2D images. Each dot represents a single cell ($n > 1000$ for each plot), with each color representing cells from independent cultures ($n > 300$ per culture). For each strain, we divided cells into 6 bins of cell size. We then normalized the values obtained with the stationary phase reporter (J45995) with those obtained by using the constitutive reporter (I7100). This normalization was necessary to remove variations in fluorescence between cells of different size that were not specific to variations in the expression of the pOsmY promoter. Our results are depicted in *e* and show no correlation between cell size and fluorescence from our stationary phase reporter. Error bars represent the standard error of the mean.

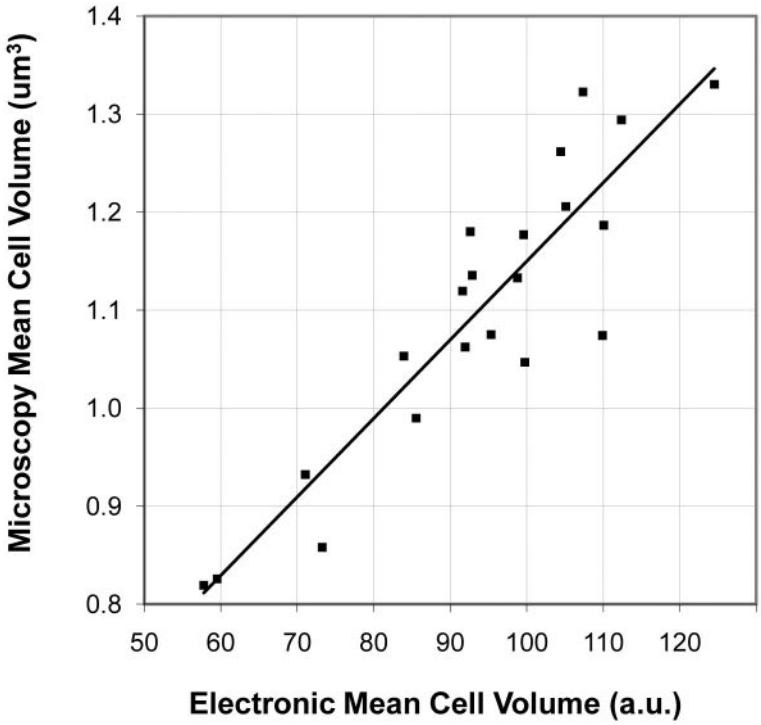

Fig. S10. Comparison of mean cell volume obtained by electronic and microscopic measurements. Mean cell volume for the 21 fractions included in Fig. 3 was obtained by microscopic and electronic measurements as described in *Experimental Procedures*. The equation of the linear trendline ($y = 0.0080x + 0.3486$) was used to convert electronic volume channel numbers into μm^3 for Fig. 2 and Fig. S4. The linear correlation between electronic and microscopy volume measurement is high ($R^2 = 0.825$).

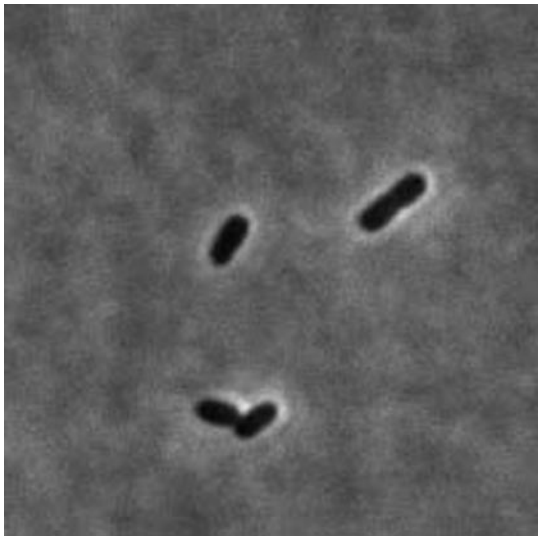

Movie S1. Lytic event and lysogeny. Two different cells are infected (producing GFP) and follow distinct fates. The larger rightmost cell is infected and becomes lytic. A smaller cell at the bottom of the field forms an apparent lysogen (i.e., the cell divides, producing fluorescent daughter cells that also divide). This movie is also shown as a filmstrip in the main text (Fig. 4 *Upper*).

Movie S1 (AVI)

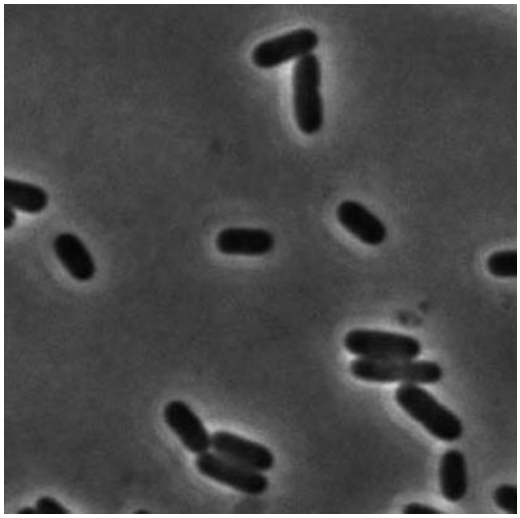

Movie S2. Lytic event. A cell in the center of the field is infected (producing GFP) and undergoes lysis.

Movie S2 (AVI)

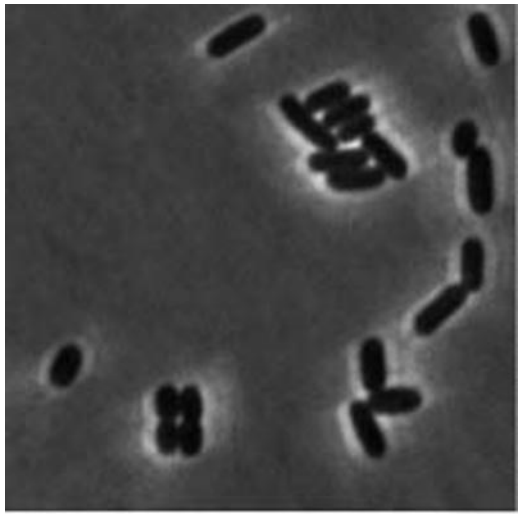

Movie S3. Mixed fate. A cell in the upper-right quadrant is infected (producing GFP), giving rise to daughter cells that obtain distinct cell fates: One daughter divides, whereas the other daughter lyses. This movie is also shown as a filmstrip in the main text (Fig. 4 *Lower*).

Movie S3 (AVI)

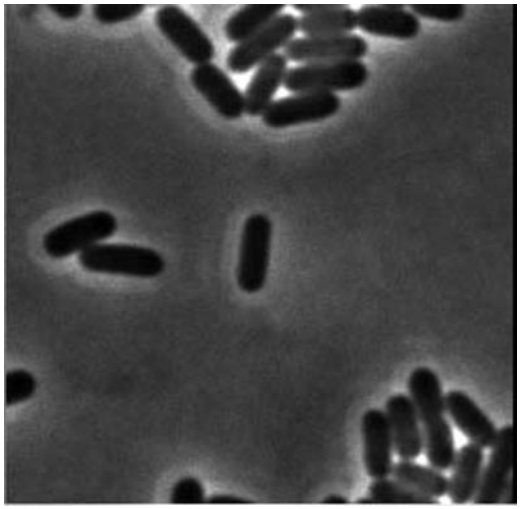

Movie S4. Dual lysis, example 1. A cell in the center of the field is infected (producing GFP), then appears to divide, giving rise to 2 daughters both of which undergo lysis.

Movie S4 (AVI)

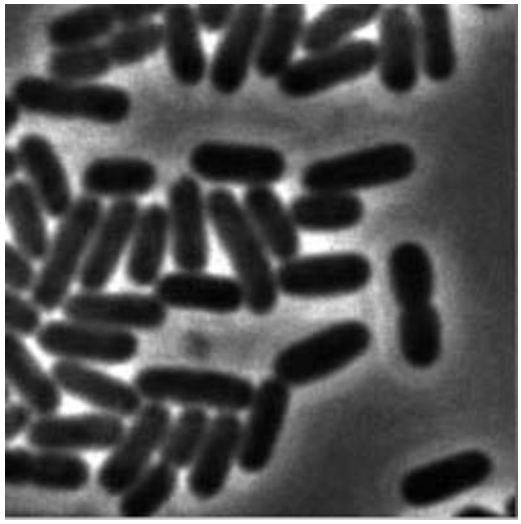

Movie S5. Dual lysis, example 2. A cell in the center of the field is infected (producing GFP), then appears to divide, giving rise to 2 daughters both of which undergo lysis.

Movie S5 (AVI)

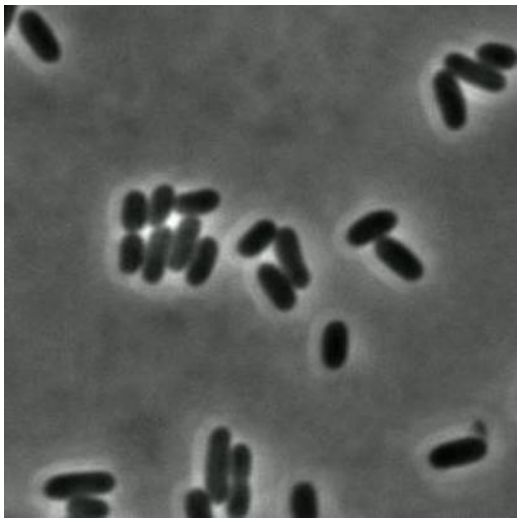

Movie S6. Mixed fate, example 2. A cell in the center of the field is infected (producing GFP), giving rise to daughter cells that obtain distinct cell fates: one daughter divides, whereas the other daughter lyses.

Movie S6 (AVI)

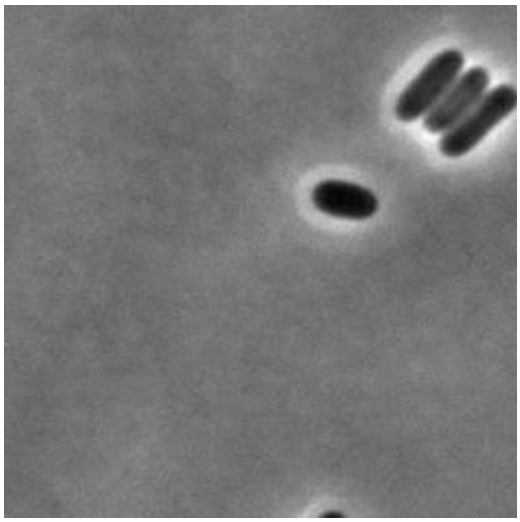

Movie S7. Mixed fate, example 3. A cell in the upper right quadrant of the field is infected (producing GFP), giving rise to daughter cells that obtain distinct cell fates: one daughter divides, whereas the other daughter lyses.

Movie S7 (AVI)

Table S1. Yield of fractions collected by counterflow centrifugal elutriation

Flow rate at which the fraction was collected, mL/min	Fraction volume, mL	Approximate yield, percentage of loaded cells collected in the fraction
6	500	1
9	500	5
10	500	6
11	500	6.5
12	500	6.5
13	100	1

We calculated a very rough estimate of the cell yield obtained at the different flow rates. Fractions produced by elutriation were concentrated ≈100-fold in 1× M9 by centrifugation. Cells from the asynchronous (unfractionated) population were also resuspended in the same medium (1× M9). The OD600 of the resulting cell suspensions was measured by using an ND-1000 spectrophotometer (NanoDrop). Assuming $1{\cdot}10^9$ colony forming units per OD600/mL for all fractions independently of mean cell volume, we calculated an estimate of the number of cells collected in each fraction. The numbers shown above represent the average of measurements made on elutriated fractions from 3 independent stationary phase cell cultures. Note that yields do not sum up to 100% of loaded cells because only collected fractions were included in this analysis.

Table S2. Elutriation system parts list

Part	Part Number
Elutriation pump*	
1. Masterflex L/S variable speed digital economy drive	1. HV-07524-50
2. Masterflex L/S 2-channel, 6-roller pump head	2. HV-07519-10
3. Masterflex L/S small cartridges (2)	3. HV-07519-85
Air purge pump*	
1. Masterflex L/S variable speed digital economy drive	1. HV-07524-50
2. Masterflex L/S Easy-Load pump head	2. HV-07518-10
3. Masterflex L/S 17 tubing (6.4 mm inside diameter), peroxide-cured	3. HV-96400-17
Masterflex pulse dampener*	HV-07596-20
Masterflex L/S 14 tubing (0.6 mm inside diameter), peroxide-cured*	HV-96400-14
3-way valves (3-way stopcocks with Luer connections, male-lock)*	HV-30600-02
JE5.0 elutriation system with large (40 mL) chamber and pressure gauge†	Contact Beckman Coulter

*Cole-Parmer Instrument Company.
†Beckman Coulter.